The Role of Carbon Dioxide During the Onset of Antarctic Glaciation

Mark Pagani, *et al.*

Science **334**, 1261 (2011);
DOI: 10.1126/science.1203909

This copy is for your personal, non-commercial use only.

If you wish to distribute this article to others, you can order high-quality copies for your colleagues, clients, or customers by clicking here.

Permission to republish or repurpose articles or portions of articles can be obtained by following the guidelines here.

The following resources related to this article are available online at www.sciencemag.org (this infomation is current as of December 2, 2011):

Updated information and services, including high-resolution figures, can be found in the online version of this article at:
http://www.sciencemag.org/content/334/6060/1261.full.html

Supporting Online Material can be found at:
http://www.sciencemag.org/content/suppl/2011/11/30/334.6060.1261.DC1.html

A list of selected additional articles on the Science Web sites **related to this article** can be found at:
http://www.sciencemag.org/content/334/6060/1261.full.html#related

This article **cites 105 articles**, 16 of which can be accessed free:
http://www.sciencemag.org/content/334/6060/1261.full.html#ref-list-1

This article appears in the following **subject collections:**
Atmospheric Science
http://www.sciencemag.org/cgi/collection/atmos

Science (print ISSN 0036-8075; online ISSN 1095-9203) is published weekly, except the last week in December, by the American Association for the Advancement of Science, 1200 New York Avenue NW, Washington, DC 20005. Copyright 2011 by the American Association for the Advancement of Science; all rights reserved. The title *Science* is a registered trademark of AAAS.

The Role of Carbon Dioxide During the Onset of Antarctic Glaciation

Mark Pagani,[1]* Matthew Huber,[2] Zhonghui Liu,[3] Steven M. Bohaty,[4] Jorijntje Henderiks,[5] Willem Sijp,[6] Srinath Krishnan,[1] Robert M. DeConto[7]

Earth's modern climate, characterized by polar ice sheets and large equator-to-pole temperature gradients, is rooted in environmental changes that promoted Antarctic glaciation ~33.7 million years ago. Onset of Antarctic glaciation reflects a critical tipping point for Earth's climate and provides a framework for investigating the role of atmospheric carbon dioxide (CO_2) during major climatic change. Previously published records of alkenone-based CO_2 from high- and low-latitude ocean localities suggested that CO_2 increased during glaciation, in contradiction to theory. Here, we further investigate alkenone records and demonstrate that Antarctic and subantarctic data overestimate atmospheric CO_2 levels, biasing long-term trends. Our results show that CO_2 declined before and during Antarctic glaciation and support a substantial CO_2 decrease as the primary agent forcing Antarctic glaciation, consistent with model-derived CO_2 thresholds.

The onset of Antarctic glaciation ~33.7 million years ago is associated with an ~+1.5 per mil (‰) shift in deep-sea benthic foraminiferal oxygen isotopic ($\delta^{18}O$) values (1), an abrupt appearance of glaciomarine sediments around the Antarctic margin (2, 3), a shift in clay mineralogy at Southern Ocean sites marking an increase in physical over chemical weathering (4, 5), a permanent deepening of the calcite compensation depth (1), and substantial high-latitude and global cooling (6, 7). Proposed causes for the abrupt onset of glaciation near the Eocene-Oligocene (E-O) boundary include a CO_2 decrease across a critical CO_2-induced temperature threshold (8), decreasing CO_2 combined with an orbital configuration that reduced polar seasonality (1, 8), and changes in regional ocean circulation and heat transport to the southern high latitudes resulting from the progressive tectonic separation of Australia and South America from Antarctica (9).

Published CO_2 reconstructions provide contradictory evidence for the role of CO_2 during high-latitude cooling and Antarctic ice sheet expansion, with alkenone-based CO_2 estimates showing a large CO_2 decline occurring 2 to 3 million years after maximum ice sheet expansion (10). Curiously, alkenone-based CO_2 estimates show an increase just before and across the E-O transition (10). In contrast, CO_2 records based on boron isotope–pH estimates from one ocean locality provide evidence for declining CO_2 levels coeval with global cooling, followed by a rebound and subsequent CO_2 decline immediately after the E-O climate event (11). Thus, existing alkenone-based CO_2 records appear to conflict with recently published boron-based CO_2 estimates, as well as our theoretical understanding of the relation between climate change and greenhouse gas forcing.

The published Cenozoic alkenone-based CO_2 record is a composite of alkenone carbon-isotopic values from both oligotrophic and eutrophic environments in the modern ocean (10). Alkenone stable carbon-isotope records from individual localities spanning the E-O climate transition are lacking and do not sample the E-O climate event in detail. Instead, published CO_2 trends for the E-O interval were inferred from analyses from Deep Sea Drilling Project (DSDP) sites 511 and 612 for the interval preceding the E-O climate transition and from DSDP sites 511, 513, and 516 and Ocean Drilling Program (ODP) site 803 for the interval after the event [supporting online material (SOM)]. Three data points from site 513, two values from site 511, and one data point from site 516 immediately follow the E-O climate transition (10). Earliest Oligocene CO_2 estimates responsible for the apparent rise in CO_2 across the E-O climate event derive from sites 511 and 513, which are presently located in poorly stratified, nutrient-rich subantarctic waters, raising the possibility that these sites do not reflect air-sea CO_2 equilibria (SOM).

For this study, we evaluated regional differences in CO_2 estimates and trends across the E-O climate transition by using the carbon-isotopic ($\delta^{13}C$) values of alkenones from six globally dispersed ocean localities, including DSDP or ODP sites 277, 336, 511, 925, 929, and 1090 (Fig. 1), representing a range of oceanographic conditions and algal-growth environments. Chronologies and sea surface temperatures (SSTs) for each site have

---

[1] Department of Geology and Geophysics, Yale University, New Haven, CT 06520, USA. [2] Earth and Atmospheric Sciences Department and the Purdue Climate Change Research Center (PCCRC), Purdue University, West Lafayette, IN 47906, USA. [3] Department of Earth Sciences, The University of Hong Kong, Hong Kong, People's Republic of China. [4] School of Ocean and Earth Science, University of Southampton, Southampton SO14 3ZH, UK. [5] Department of Earth Sciences, Uppsala University, SE-75 236 Uppsala, Sweden. [6] Climate Change Research Centre, Faculty of Science, University of New South Wales, Sydney 2052, Australia. [7] Department of Geosciences, University of Massachusetts-Amherst, Amherst, MA 01003, USA.

*To whom correspondence should be addressed. E-mail: mark.pagani@yale.edu

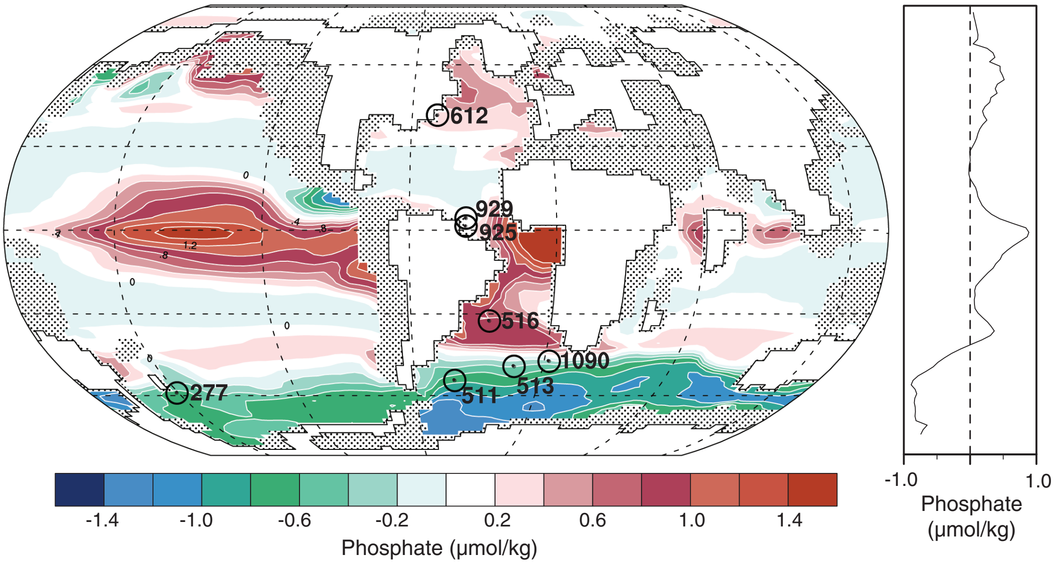

Fig. 1. DSDP and ODP sites used in this study overlain on model-derived surface ocean phosphate concentration anomaly. Sites are rotated back to their late Eocene paleopositions. (**Left**) Contours indicate anomalies of the UVic climate–ecosystem–carbon cycle model-predicted surface ocean phosphate concentration (late Eocene simulation minus modern simulation; SOM). Modern continents are indicated by stippling, and Eocene continents are white with black outline. (**Right**) Zonal mean phosphate anomalies. Late Eocene continental configuration is associated with greatly reduced Southern Ocean phosphate and increased tropical and Northern Hemisphere phosphate.

been previously established (*6*) or updated for this study (SOM).

Alkenones are long-chained (C_{37} to C_{39}) unsaturated ethyl and methyl ketones exclusively produced by haptophyte algae (*12*). Alkenone-based CO_2 reconstructions derive from the stable carbon-isotope composition of the di-unsaturated C_{37} methyl ketone ($\delta^{13}C_{37:2}$) and the total carbon-isotope fractionation that occurred during algal growth ($\varepsilon_{p37:2}$) (SOM). Nutrient-limited chemostat cultures show that $\varepsilon_{p37:2}$ values vary with the concentration of aqueous CO_2 ($[CO_{2aq}]$), specific growth rate, and cell geometry (*13*). Dilute batch cultures with nutrient-replete conditions produce substantially lower $\varepsilon_{p37:2}$ values, a different relationship for ε_p versus μ/CO_{2aq}, a relatively minor response to $[CO_{2aq}]$ (*14*), and an irradiance effect (*15*). Concentrations of reactive soluble phosphate ($[PO_4^{3-}]$) are necessary to estimate $[CO_{2aq}]$ from $\varepsilon_{p37:2}$ values (*10*, *16*) (SOM). This relationship with $[PO_4^{3-}]$ reflects differences in rates of carbon fixation, but it is unlikely that $[PO_4^{3-}]$ by itself is responsible for the variability in carbon fixation rates. Instead, it is generally assumed that the availability of other biolimiting micronutrients that display distributions similar to phosphate also affects the growth characteristics of these populations, whereas $[PO_4^{3-}]$ acts as a proxy for these other variables. Despite these complexities, a study of Pacific Ocean sediments demonstrates that the alkenone methodology resolves relatively small differences in water-column $[CO_{2aq}]$ when SSTs and $[PO_4^{3-}]$ are reasonably constrained (*16*). For this work, we calculated $[CO_{2aq}]$ at each site assuming maximum haptophyte production occurred between 30 and 50 m depths and applied the average $[PO_4^{3-}]$ determined from modern mean-annual phosphate depth profiles and paleo-estimates from model simulations at each paleo-location (SOM). SST was determined by using temperature proxies $U_{37}^{K'}$ (alkenone unsaturation index) and TEX_{86} (tetraether index) (*6*) (SOM). A sensitivity analysis for proxy temperatures was performed by using climate model–derived SSTs as an alternative to proxy interpretations.

Our $\delta^{13}C_{37:2}$ analyses provide evidence for the persistence of two distinct, isotopic groupings (Fig. 2A). Higher $\delta^{13}C_{37:2}$ values characterize Northern Hemisphere sites, the equatorial region, and southern subtropics; whereas lower $\delta^{13}C_{37:2}$ values are associated with sites located in subantarctic and Antarctic waters. $\varepsilon_{p37:2}$ values, which eliminate the isotopic influence of inorganic aqueous carbon used during photosynthesis, reduce differences between Antarctic/subantarctic sites and more northerly sites, but distinct regional isotopic offsets persist (Fig. 2B).

Reconstructed CO_2 estimates using proxy temperatures and modern nutrient distributions (*10*) show stark differences among sites (Fig. 3A). Specifically, all Antarctic and subantarctic sites are characterized by substantially higher CO_2 estimates as well as CO_2 offsets in comparison to low-latitude sites 925 and 929. These offsets that are implausible either by analogy to modern CO_2 disequilibrium distributions or by those generated by our Eocene modeling that indicate Southern Ocean sites maintained CO_2 values between 1 and 200 parts per million (ppm) lower than atmospheric values (SOM). Most sites show evidence of CO_2 decline across the E-O climate transition (SOM). However, a compilation of CO_2 records with Antarctic and subantarctic data included renders an indeterminable evaluation of atmospheric CO_2 concentration and its relationship to the E-O climate shift (Fig. 3A).

Regionally higher surface-water $[CO_{2aq}]$ at Antarctic/subantarctic sites compared to other sites is qualitatively implied by relatively higher Antarctic/subantarctic $\varepsilon_{p37:2}$ values. Another approach to qualitatively evaluate regional CO_2 differences is through an analysis of cell-size differences of ancient alkenone producers. Previous work interpreted substantial reductions in cell-size dimensions of alkenone-producing coccolithophores across the E-O climate transition as a response to CO_2 limitation during carbon fixation (*17*). Our new cell-size measurements indicate that alkenone-producing algae from Antarctic/subantarctic sites were larger compared to more northerly sites (SOM). Smallest mean cell diameters are found in the equatorial Atlantic, where small and medium-sized (3 to 7 μm) reticulofenestrids and *Cyclicargolithus* dominated. By contrast, the abundance of large reticulofenestrids (including *Reticulofenestra umbilica* and *R. bisecta*) was significantly higher in the Antarctic/subantarctic (SOM). Theory argues that cell geometry differences should directly affect the magnitude of $\varepsilon_{p37:2}$ values (*13*). However, if differences in cell geometry were primarily responsible for the expression of carbon-isotopic compositions, relatively lower $\varepsilon_{p37:2}$ values would be predicted from Antarctic/subantarctic sites (*13*, *17*), in contrast to what is observed (Fig. 2B). Instead, it is more likely that differences in cell geometry reflect higher $[CO_{2aq}]$, lower algal growth rates (perhaps because of low nutrient flux), or a combination of both at southern sites (*17*) (SOM).

In addition to cell size, CO_2 estimates determined from $\varepsilon_{p37:2}$ rely on various assumptions including the value for the carbon isotope fractionation associated with carbon fixation (ε_f), SST, and $[PO_4^{3-}]$. An ε_f value of 29‰ is widely accepted for the in vitro fractionation due to RuBisCO (ribulose-1,5-bisphosphate carboxylase-oxygenase) (*18*, *19*). However, smaller in situ fractionations ranging from 25 to 28‰ are attributed to the effects of other enzymes, such as the β-carboxylase (phosphoenolpyruvate-carboxylase) (*13*, *15*, *20*, *21*). Considering that β-carboxylation is responsible for bicarbonate uptake, it is possible that its expression was greatly reduced by higher ambient CO_2 levels, leading to higher ε_f values. Application of higher ε_f values substantially reduces calculated regional CO_2 offsets (Fig. 3B) (SOM). In comparison with other variables, the value of ε_f constitutes the most important lever on the magnitude of CO_2 estimates, particularly as $\varepsilon_{p37:2}$ approaches the value of ε_f applied in the calculation of CO_2 (Fig. 3, B, D, and F).

Proxy SST values ($U_{37}^{K'}$ and TEX_{86}) used in this study are subject to uncertainty, given difficulties in determining diagenetic alterations and modifications to modern empirical calibrations because of evolutionary, ecological, and physical oceanographic changes with time. For example, Eocene temperature reconstructions from the

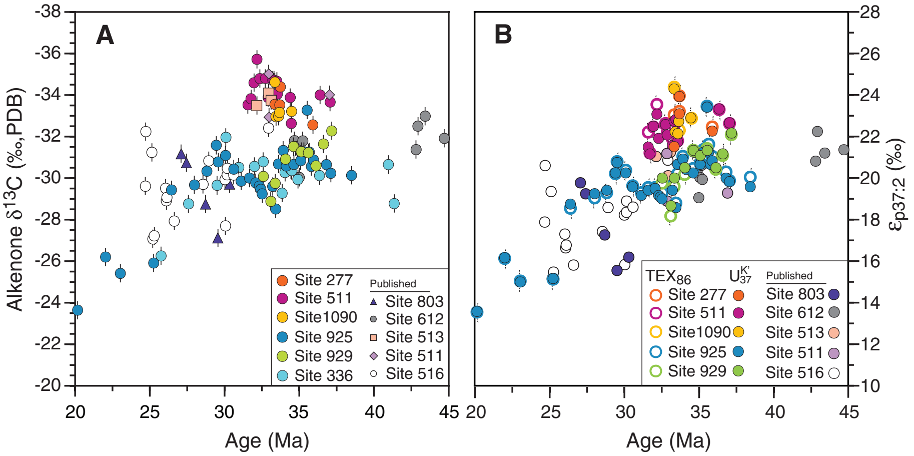

Fig. 2. Compilation of isotopic compositions of di-unsaturated alkenones and $\varepsilon_{p37:2}$ values. (**A**) Carbon-isotopic compositions of di-unsaturated alkenones. Analytical accuracy of carbon isotope measurements is ±0.2‰ (root mean square error) on the basis of an *n*-C_{20} alkane standard injected daily. Standard error, represented by the error bars, was ±0.4‰ or better. (**B**) $\varepsilon_{p37:2}$ values calculated by using foraminiferal carbonate $\delta^{13}C$ values and temperature estimates (SOM) from both $U_{37}^{K'}$ and TEX_{86}. Previous published data from (*10*). Site 336 lacks carbonates necessary for the calculation of $\varepsilon_{p37:2}$. Ma indicates million years ago.

southwest Pacific (*22*) imply meridional temperature gradients and high-latitude zonal temperature gradients (*23*) that are difficult to explain by known ocean-atmosphere physics or other published records (*23*, *24*). It is noteworthy that model simulations of Eocene climates indicate substantially lower temperatures for the southwest Pacific high-latitude site evaluated in this work (SOM), although they are generally in agreement at most other high-latitude ocean localities (*6*), as well as with terrestrial paleoclimate records (*23*). If we assume model SSTs are valid, calculated CO_2 offsets between sites are also substantially reduced (Fig. 3C). Indeed, spurious proxy temperatures could prove to be the critical impediment in advancing our understanding of ancient climate systems, given their importance in our evaluation of all other aspects of ocean and atmospheric dynamics in addition to CO_2 estimates.

High [PO_4^{3-}] applied to Antarctic/subantarctic sites derives from modern water-column nutrient distributions (SOM), assuming that Eocene-Oligocene circulation was similar to today. This is likely a poor assumption, because the modern upwelling of deep, nutrient-rich Southern Ocean water relies on the presence of a deep channel at the latitudes of the Drake Passage. In the absence of a deep circum-Antarctic circulation during the Eocene (*25*), upwelling must have come from shallower depths (*26*, *27*) and limiting nutrient concentrations were lower. To demonstrate that this is the case, we ran a present-day and an Eocene configuration of the UVic Earth system model of intermediate complexity, including a marine ecosystem and full carbon cycle (SOM). Nutrient cycles are free to evolve, and present-day simulations agree favorably with modern observations (SOM). In accordance with ocean circulation theory, our Eocene modeling results show that upwelling from the abyss was weaker in the Southern Ocean, forcing older, high-phosphate waters to upwell elsewhere and leading to lower mixed-layer nutrient concentrations in the Southern Ocean (Fig. 1). Therefore, the application of present-day [PO_4^{3-}] (and the implicit assumption of high haptophyte growth rates) is likely a poor choice on the basis of known changes in paleobathymetry and the well-established physical oceanographic and nutrient flux responses they engender.

Application of simulated [PO_4^{3-}] also helps to reduce CO_2 offsets (Fig. 3E) but, similar to the effect of temperature, still fails to completely eliminate higher CO_2 distributions in the high-southern latitudes. Higher [CO_{2aq}] in these regions is unsupported by our model results (SOM) but supported by one interpretation of our cell-size analysis, and so the persistence of an offset is not inconsistent with the totality of proxy data. Alternatively, whereas cell-size trends imply a temporal decrease in [CO_{2aq}], regional cell-size differences could reflect spatial differences in nutrient limitation (*17*) and very low haptophyte growth rates in the high-southern regions, which promoted higher $\varepsilon_{p37:2}$ values, consistent with model results.

Uncertainties in the magnitude of ε_f, [PO_4^{3-}], and temperature values compromise the efficacy

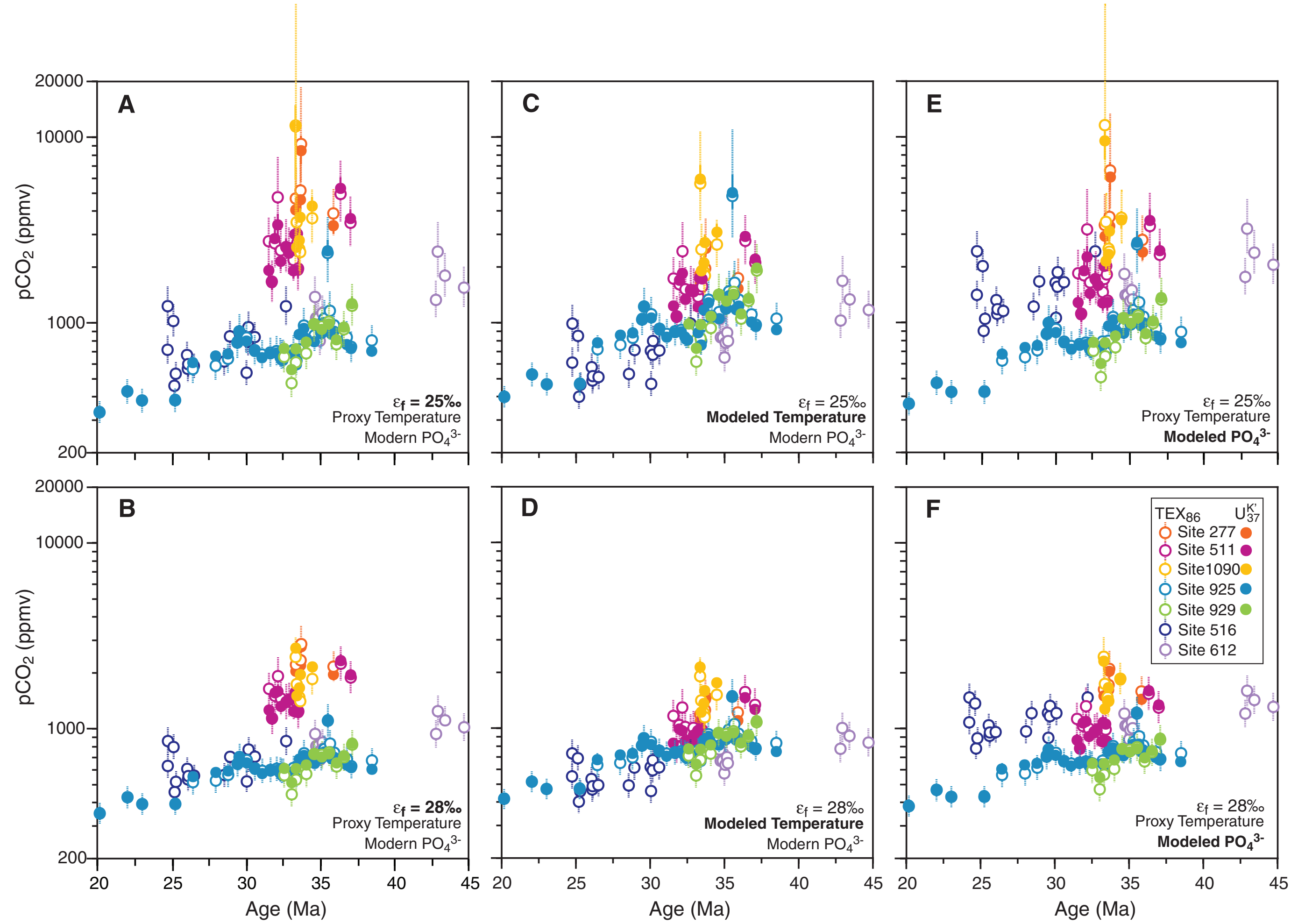

Fig. 3. Calculated p_{CO_2} from $\varepsilon_{p37:2}$ values. Error bars associated with each point reflect the uncertainty in CO_2 because of the temperature uncertainties for each temperature proxy. (**A**) p_{CO_2} calculated by using $U^{K'}_{37}$ and TEX_{86} values, assuming ε_f = 25‰ and using modern [PO_4^{3-}] averaged between 30 and 50 m for each paleolocation (SOM). (**B**) Same as (A) but using an ε_f = 28‰. (**C**) Same as (A) but using modeled temperatures averaged between 30 and 50 m for each paleolocation (SOM). (**D**) Same as (C) but using an ε_f = 28‰. (**E**) Same as (A) but using modeled [PO_4^{3-}] averaged between 30 and 50 m for each paleolocation (SOM). (**F**) Same as (E) but using an ε_f = 28‰.

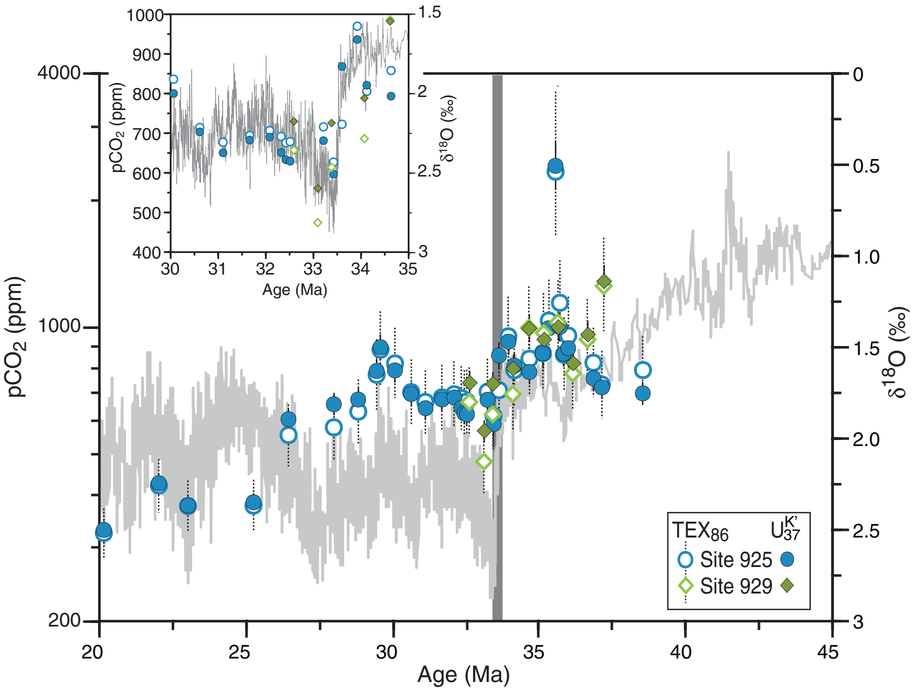

Fig. 4. Reconstructed $p\text{CO}_2$ records from low-latitude sites 925 and 929. Calculations apply $\varepsilon_f = 25‰$ and modern $[\text{PO}_4^{3-}]$ at paleolocations (SOM). Error bars associated with each point reflect the uncertainty in CO_2 because of temperature uncertainties for each temperature proxy. Gray line represents a compilation of $\delta^{18}\text{O}$ values of benthic foraminifera (*30*).

of the alkenone proxy at southern high-latitude localities in this study, with the potential to greatly overestimate CO_2 levels and obfuscate global temporal CO_2 variations when included in global compilations. Importantly, other published CO_2 results from equivalent localities (*28*) could reflect similar biases and offsets. In contrast, these effects are substantially reduced across low-latitude sites, where uncertainties in temperature and nutrient input are smaller and the lower magnitude of ε_p diminishes the range of CO_2 uncertainty. Accordingly, we focus on CO_2 reconstructions derived from low-latitude sites 925 and 929 and apply modern phosphate concentrations at each paleolocation.

Low-latitude records show a persistent CO_2 decline beginning about two million years before the onset of rapid cooling 33.7 million years ago (Fig. 4) that continues just beyond the climate event. Site 925 data suggest CO_2 increased somewhat before cooling; however, corroborating results from site 929 are lacking. Site 925 also shows an increase in CO_2 during the mid-Oligocene that tracks warming inferred from benthic $\delta^{18}\text{O}$ values (Fig. 4), a pattern corroborated by $\varepsilon_{p37:2}$ trends from site 336 (Fig. 2A). A long-term lowering of CO_2 during the Oligocene is consistent with early Miocene CO_2 reconstructions from other localities (*10*), but our sensitivity analysis allows for higher early Miocene CO_2 levels relative to previously published results if $[\text{PO}_4^{3-}]$ and temperature estimates were higher than originally assumed.

The decline in the partial pressure of atmospheric carbon dioxide during the E-O climate event was substantial, but absolute CO_2 concentrations depend on the value of ε_f applied. Collectively, CO_2 estimates calculated by using $U^{K'}_{37}$ and TEX_{86} SST estimates and a range of ε_f values indicate that CO_2 decreased ~40% from 35.5 to 32.5 million years ago (SOM). Application of reasonable ε_f values (25 to 28‰) indicates that the partial pressure of atmospheric CO_2 fell from 1200 to 1000 ppm to 700 to 600 ppm. Interestingly, the change in CO_2 determined from this study, as well as the boron-isotope methodology (*11*), is consistent with model estimates for a threshold CO_2 level required for rapid Antarctic glaciation (*8*, *29*).

We conclude that the available evidence supports a fall in CO_2 as a critical condition for global cooling and cryosphere evolution ~34 million years ago. Whether CO_2 acted alone to cause the E-O transition or whether a threshold CO_2 level in combination with favorable orbital configurations (*1*) ultimately triggered glaciation cannot be determined from our results. However, during the E-O transition both CO_2 decline and enhanced ice albedo account for global temperature changes. Lastly, the long-term permanence of the CO_2 decline (*10*) and the impermanent inorganic carbon isotope shift (*1*) implicate the role of silicate weathering rates over the influence of short-term organic-carbon burial rates as the primary cause for long-term change in atmospheric carbon dioxide.

References and Notes

1. H. K. Coxall, P. A. Wilson, H. Pälike, C. H. Lear, J. Backman, *Nature* **433**, 53 (2005).
2. M. J. Hambrey, B. Larsen, W. U. Ehrmann, *Proc. Ocean Drill. Program, Sci. Results* **119**, 77 (1991).
3. M. J. Hambrey, P. J. Barrett, in *The Antarctic Paleoenvironment: A Perspective on Global Change, Part 2*, J. P. Kennett, D. A. Warnke, Eds. (vol. 60 of Antarctic Research Series, American Geophysical Union, Washington, DC, 1993), pp. 91–124.
4. W. U. Ehrmann, *Proc. Ocean Drill. Program, Sci. Results* **119**, 185 (1991).
5. C. Robert, J. P. Kennett, *Geology* **25**, 587 (1997).
6. Z. Liu *et al.*, *Science* **323**, 1187 (2009).
7. J. S. Eldrett, D. R. Greenwood, I. C. Harding, M. Huber, *Nature* **459**, 969 (2009).
8. R. M. DeConto, D. Pollard, *Nature* **421**, 245 (2003).
9. J. P. Kennett, *J. Geophys. Res.* **82**, 3843 (1977).
10. M. Pagani, J. C. Zachos, K. H. Freeman, B. Tipple, S. Bohaty, *Science* **309**, 600 (2005); 10.1126/science.1110063.
11. P. N. Pearson, G. L. Foster, B. S. Wade, *Nature* **461**, 1110 (2009).
12. M. H. Conte, J. K. Volkman, G. Eglinton, in *The Haptophyte Algae*, J. C. Green, B. S. C. Leadbeater, Eds. (Clarendon, Oxford, 1994), pp. 351–377.
13. B. N. Popp *et al.*, *Geochim. Cosmochim. Acta* **62**, 69 (1998).
14. U. Riebesell, A. T. Revill, D. G. Holdsworth, J. K. Volkman, *Geochim. Cosmochim. Acta* **64**, 4179 (2000).
15. B. Rost, I. Zondervan, U. Riebesell, *Limnol. Oceanogr.* **47**, 120 (2002).
16. M. Pagani, K. H. Freeman, N. Ohkouchi, K. Caldeira, *Paleoceanography* **17**, 1069 (2002).
17. J. Henderiks, M. Pagani, *Earth Planet. Sci. Lett.* **269**, 576 (2008).
18. C. A. Roeske, M. H. O'Leary, *Biochemistry* **23**, 6275 (1984).
19. J. A. Raven, A. M. Johnston, *Limnol. Oceanogr.* **36**, 1701 (1991).
20. R. Goericke, J. P. Montoya, B. Fry, in *Stable Isotopes in Ecology*, K. Lajtha, B. Michener, Eds. (Blackwell Scientific, Boston, 1994), pp. 187–221.
21. G. D. Farquhar, P. A. Richards, *Aust. J. Plant Physiol.* **11**, 539 (1984).
22. C. J. Hollis *et al.*, *Geology* **37**, 99 (2009).
23. M. Huber, R. Caballero, *Clim. Past* **7**, 603 (2011).
24. P. K. Bijl *et al.*, *Nature* **461**, 776 (2009).
25. P. F. Barker, E. Thomas, *Earth Sci. Rev.* **66**, 143 (2004).
26. J. R. Toggweiler, H. Bjornsson, *J. Quat. Sci.* **15**, 319 (2000).
27. W. P. Sijp, M. H. England, J. R. Toggweiler, *J. Clim.* **22**, 6639 (2009).
28. P. K. Bijl *et al.*, *Science* **330**, 819 (2010).
29. R. M. DeConto *et al.*, *Nature* **455**, 652 (2008).
30. J. C. Zachos, M. Pagani, L. Sloan, E. Thomas, K. Billups, *Science* **292**, 686 (2001).

Acknowledgments: This work was supported by a postdoctoral fellowship provided by Yale University Department of Geology and Geophysics, with funding provided by the NSF under awards OCE-0902882, OCE-0902993, EAR-0628358, ATM-0513402, ATM-0927946, and ANT-034248. This is PCCRC publication number 1115. Natural Environment Research Council grant NE/G003270/1 provided funds for the stable isotope analysis of carbonates. J.H. was funded by the Royal Swedish Academy of Sciences (KAW 2009.0287).

Supporting Online Material

www.sciencemag.org/cgi/content/full/334/6060/1261/DC1
Materials and Methods
SOM Text
Figs. S1 to S15
Tables S1 to S6
References (*31–112*)

7 February 2011; accepted 13 October 2011
10.1126/science.1203909